Evaluation and improvement of IEC 60891 correction methods for I-V curves of defective photovoltaic panels

Baojie Li, Anne Migan-Dubois, Claude Delpha, Demba Diallo

▶ **To cite this version:**

Baojie Li, Anne Migan-Dubois, Claude Delpha, Demba Diallo. Evaluation and improvement of IEC 60891 correction methods for I-V curves of defective photovoltaic panels. Solar Energy, 2021, 216, pp.225-237. 10.1016/j.solener.2021.01.010 . hal-03237596

HAL Id: hal-03237596
https://centralesupelec.hal.science/hal-03237596

Submitted on 4 Nov 2021

Evaluation and Improvement of IEC 60891 Correction Methods for I-V Curves of Defective Photovoltaic Panels

Baojie LI[1,2], Anne MIGAN-DUBOIS[1], Claude DELPHA[2], Demba DIALLO[1*],

[1] Université Paris-Saclay, CentraleSupélec, CNRS, GeePs, Sorbonne Université, 3-11 Rue Joliot Curie, Gif Sur Yvette, 91192, France
[2] Université Paris-Saclay, CNRS, CentraleSupélec, L2S, 3 Rue Joliot Curie, Gif Sur Yvette, 91192, France
* Corresponding author: demba.diallo@centralesupelec.fr

Abstract: Correction of the I-V curve permits the comparison of curves measured under different conditions for photovoltaic (PV) panels' health monitoring purpose. IEC 60891 has defined three standard procedures named 1, 2 and 3 for the correction. They were initially designed to correct the curves of healthy PV panels. However, their performance, when applied to I-V curves measured on faulty panels, is rarely discussed. This work evaluates these correction methods on I-V curves simulated under different environmental conditions and for five types of defects of varying severity. The results show that procedure 3 has a relatively better overall performance but is not suitable for rapid application in the field as it requires the determination of reference curves. It is found that procedures 1 and 2 could introduce distortion of the curve's shape, with a relative error of up to 13.8 % and 6.4 %, respectively. A misestimation of 9.1 % for key parameters of the curve has been observed, when using procedure 2 for maximum power. Based on the performance analysis, a new correction method is proposed to fit the corrected voltage. It can reduce the curve's average correction error by 31.3 % compared to the original single curve correction method. Challenges and directions for future work are also presented.

Key words: Photovoltaic; I-V curve; I-V curve correction; IEC 60891; Fault detection and diagnosis;

Nomenclature			
a	Irradiance correction factor	V_{oc}^{real}	V_{OC} of real curve at STC (V)
α	Absolute temperature coefficient of I_{SC} (A/°C)	V_{rp}	Voltage of inflexion point under PS (V)
α_{rel}	Relative temperature coefficient of I_{SC} (%/°C)	PS	Partial shading
β	Absolute temperature coefficient of V_{OC} (V/°C)	P_m	Maximum Power (W)
β_{rel}	Relative temperature coefficient of V_{oc} (%/°C)	PV	Photovoltaic
CE	Curve error (%)	OC	Open circuit
G	Global in-plane irradiance (W/m^2)	RE	Relative error (%)
$GainPS$	Block gain used in simulation to control PS degree	R_{OC}	Resistance used in simulation for OC (Ω)
I	Current (A)	R_s	Series resistance (Ω)
I^c	Current of corrected curve (A)	R_{s_degra}	Resistance used in simulation for Rs degradation (Ω)
I^{real}	Current of real curve at STC (A)		
I_{MPP}	Current at MPP (A)	R_{SC}	Resistance used in simulation for SC (Ω)
I_{rp}	Current of inflexion point under PS (A)	R_{sh}	Shunt resistance (Ω)
I_{SC}	Short-circuit current (A)	R_{sh_degra}	Resistance used in simulation for Rsh degradation (Ω)
I_{SC}^{real}	I_{SC} of real curve at STC (A)		
I-V curve	Current-voltage characteristics	SC	Short circuit
MPP	Maximum power point	STC	Standard test condition
κ	Curve correction factor	TC	Temperature coefficient
V	Voltage (V)	Tm	Module temperature (°C)
V_{MPP}	Voltage at MPP (V)	γ	Interpolation constant for correction method M3
V_{OC}	Open-circuit voltage (V)		
V_{OC}^{STC}	V_{OC} under STC in healthy condition (provided in datasheet) (V)		

1. Introduction

The current-voltage characteristics (I-V curves) measured from a faulty photovoltaic (PV) module or array (from now on, termed as faulty I-V curve) contain valuable information on the health status (Fadhel et al., 2019; Li et al., 2019). For a single module or small-scale PV string, one I-V tracer device can measure I-V curves under various meteorological conditions (Sarikh et al., 2020; Zhu and Xiao, 2020). Hardware solutions (integrated at inverter level) (Spataru et al., 2015) support are now commercially available to measure I-V curves at array or power plant level (Huawei, 2020). Therefore, with the increasing availability of field-measured I-V curves, I-V curves for PV health monitoring are becoming a hot topic (Mellit et al., 2018; Pillai and Rajasekar, 2018).

Based on a field-measured I-V curve under any environmental conditions, there are two common ways (Mellit et al., 2018; Pillai and Rajasekar, 2018) to use it for PV health monitoring and diagnosis:

- *Model-based difference analysis*: Analyze the residue between the measured I-V curve (or the extracted features) and the simulated ones for identical environmental condition,

- *Correction-based analysis*: Correct the whole measured I-V curve (or the extracted features) to specific environmental condition (generally Standard Test Condition (STC) (1000 W/m^2 and 25 °C)).

It is clear that for a model-based difference analysis, it is unnecessary to correct the I-V curve, but a suitable and accurate PV model is required.

However, for correction-based analysis, correction of the I-V curve is an indispensable step to make curves measured under different environmental conditions comparable. Based on the corrected curves, the open-circuit voltage (V_{OC}), short-circuit current (I_{SC}), the voltage at the point of maximum power (V_{MPP}), current (I_{MPP}) and power (P_m) are commonly extracted characteristics for fault diagnosis (Agrawal et al., 2020; Chen et al., 2017; Huang et al., 2019) or power loss analysis (Wang et al., 2020). Besides, equivalent series resistance (R_s) or shunt resistance (R_{sh}) are also commonly calculated from corrected curves to analyze the degradation mode of PV networks (Bouaichi et al., 2019; Silva et al., 2019).

In this sense, if there are significant errors in the corrected curves or the corresponding characteristics, the subsequent PV diagnosis's accuracy will be severely compromised. Therefore, correction of I-V curves plays a vital role in PV health monitoring.

There are no specific methods proposed for the correction of faulty I-V curves to the best of our knowledge. Consequently, most researchers adopt the original or simplified IEC 60891 (IEC 60891, 2009) correction procedures (Golive et al., 2019; Rajput et al., 2016). For example, several authors have adopted the procedure 1 in IEC 60891 to correct I-V curves measured under partial shading (PS) (Dolara et al., 2013), potential induced degradation (PID) (Martínez-Moreno et al., 2018), dust soiling (Tanesab et al., 2017, 2015), or hot spot (Ma et al., 2019). Besides, procedure 2 of IEC 60891 is also used to correct the I-V curves' key parameters (Chen et al., 2017). These parameters can then be used as inputs of a classifier (e.g., artificial neural network (ANN)) to automatically identify the fault types (PS, open circuit (OC), short circuit (SC), or shunt resistance degradation). Similar applications can also be found in (Zhu et al., 2018).

It should be noted that these methods based on the IEC 60891 standard have been all initially designed for the correction of curves measured from healthy PV panels. Moreover, in literature, the suitability of these methods correction of the I-V curves of defective panels is rarely studied, let alone whether the defects' characteristics are distorted by the correction and thus lead to a diagnostic error. All these issues are decisive for the diagnosis of PV faults (Triki-Lahiani et al., 2018). Thus, this paper aims to first evaluate the IEC 60891 methods' performance for the correction of faulty panels I-V curves. Then, based on IEC 60891 methods' performance analysis, an improved correction method will be proposed and evaluated.

The outline of the paper is as follows. Section 2 introduces the methodology from the simulation of faulty I-V curves, introduces the correction methods and performance evaluation metrics. Sections 3 and 4 present the correction performance using the single or multiple-curves-based methods, respectively. The comparison of these methods and guidance on future work are discussed in Section 5. Section 6 concludes the paper.

2. Methodology for the evaluation of correction methods

Since our target is to evaluate the error caused by the correction methods, it is essential to avoid the effects of other factors, like the measurement uncertainty on irradiance G, module temperature Tm and I-V curve, which could be up to 5 % (Friesen et al., 2018). Therefore, the curves to be corrected are generated in simulation rather than from field measurement to ensure all the correction formula parameters are real values, without any bias.

2.1. Simulation of I-V curves

2.1.1. Simulation model

A PV array is modelled under Simulink® to address several fault types. The array consists of two strings in parallel, and each string of three mc-Si modules in series, as shown in Fig.1 (a). Each module comprises three strings of twenty cells and three bypass diodes, as shown in Fig.1 (b). Table 1 lists the detailed module parameters.
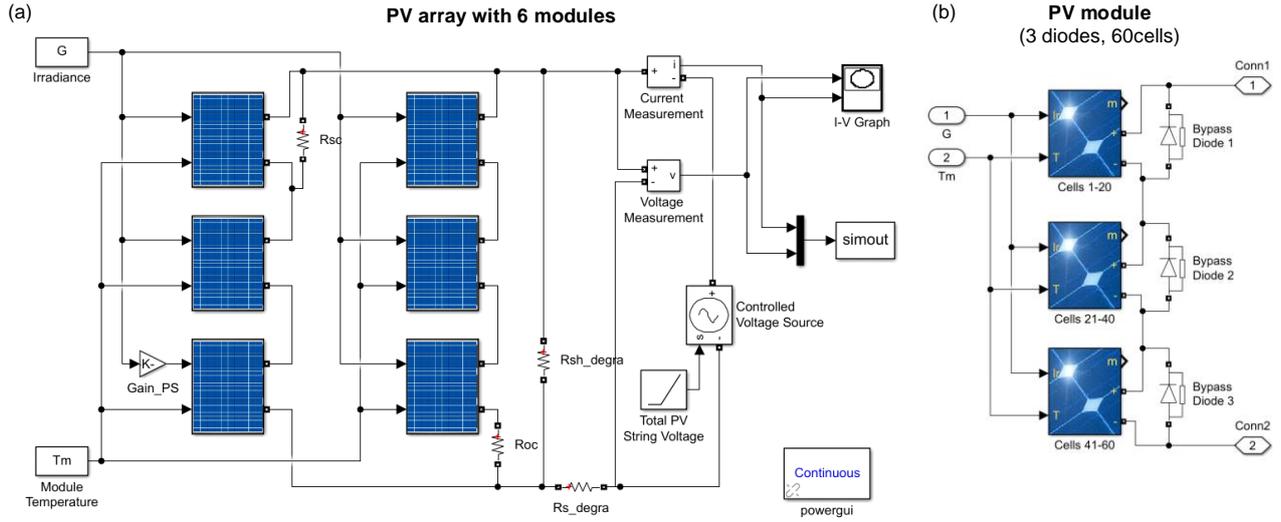
Fig. 1 Simulation model: (a) PV array structure, (b) PV module structure

Table 1 Parameter setting of mc-Si PV module

Variable	Value	Variable	Value
I_{SC}	8.64 A	V_{MPP}	31.80 V
V_{OC}	37.90 V	α_{rel}	0.02 %/°C
I_{MPP}	6.52 A	β_{rel}	-0.36 %/°C

where, α_{rel} and β_{rel} are the temperature coefficients (TC) of I_{SC} and V_{OC}, respectively.

The characteristics of the array's I-V curve depend on:

- *G* and *Tm*: the values are identical for all the modules and depend on the correction methodology, which will be detailed in Sections 3.1 and 4.1;

- Fault Parameters: the gain block and resistors added as shown in Figure 1 (a), which are detailed as follows.

2.1.2. Configuration of faults

With the gain block and the additional resistors, the model can simulate PV array under healthy and faulty conditions. In this work, five typical faults are considered:

1) Partial shading (PS): 1 module is shaded by adjusting the value of the GainPS coefficient which varies in the range [0, 1] and controls the irradiation of the module ;

2) Short-Circuit (SC): 1 module is short-circuited by connecting the resistance R_{SC} in parallel;

3) Open-Circuit (OC): 1 string is open-circuited, by connecting the resistance R_{OC} in series;

4) Rs degradation (Rs degra): the equivalent series resistance of the array is increased by putting in series additional resistance R_{s_degra};

5) Rsh degradation (Rsh degra): the equivalent shunt resistance of the array is decreased by connecting in parrallel the resistance R_{sh_degra};

Table 2 summarizes the different fault parameters and their corresponding range of variation used to analyze the impact of fault severity on the correction performance, presented in sections 3.2 and 4.2.

Table 2 Parameter setting for the different conditions

Condition	GainPS	R_{SC} (Ω)	R_{OC} (Ω)	R_{s_degra} (Ω)	R_{sh_degra} (Ω)
Healthy	1	10^5	10^{-5}	10^{-5}	10^5
PS 1 module	**[0-1]**	10^5	10^{-5}	10^{-5}	10^5
SC 1 module	1	**10^{-5}**	10^{-5}	10^{-5}	10^5
OC 1 string	1	10^5	**10^5**	10^{-5}	10^5
Rs degradation	1	10^5	10^{-5}	**[10^{-5}-2]**	10^5
Rsh degradation	1	10^5	10^{-5}	10^{-5}	**[10^5-10]**

2.2. Correction methods

Through the literature review, the most common I-V curve correction methods are based on three procedures (hereafter, called M1, M2, and M3) proposed in IEC 60891 (IEC 60891, 2009). These methods and a proposed M2-based improved method are detailed as follows:

- Method 1 (M1):

$$I_2 = I_1 + I_{SC1}(G_2/G_1 - 1) + \alpha(T_{m2} - T_{m1}) \qquad (1)$$

$$V_2 = V_1 - R_s(I_2 - I_1) - \kappa I_2(T_{m2} - T_{m1}) + \beta(T_{m2} - T_{m1}), \qquad (2)$$

where, I_1 and I_2, V_1 and V_2, T_{m1} and T_{m2}, G_1 and G_2 are the current, voltage, module temperature, and irradiance before, and after correction, respectively; I_{SC1} is the short-circuit current before correction; α and β are the PV module absolute TC of I_{SC} and V_{OC}, respectively; $\alpha = \alpha_{rel} \cdot I_{SC}^{STC}$, $\beta = \beta_{rel} \cdot V_{OC}^{STC}$, α_{rel} and β_{rel} are the relative TC of I_{SC} and V_{OC} (presented in Table 1); R_s is the internal series resistance and κ is the curve correction factor.

- Method 2 (M2):

$$I_2 = I_1\big(1 + \alpha_{rel}(T_{m2} - T_{m1})\big)G_2/G_1 \qquad (3)$$

$$V_2 = V_1 + V_{OC1}[\beta_{rel}(T_{m2} - T_{m1}) + a \cdot ln(G_2/G_1)] - R_s(I_2 - I_1) - \kappa \cdot I_2(T_{m2} - T_{m1}), \qquad (4)$$

where, V_{OC1} is the V_{OC} before correction; a is the irradiance correction factor; R_s and κ are determined by the procedure described in (IEC 60891, 2009).

The determination of the coefficients a, R_s and κ for M1 and M2 requires a group of I-V curves at the same G or at the same Tm, which is troublesome and time-consuming to fulfill in real life. Therefore, in most M1 and M2 applications, these coefficients are either tuned via simulation under healthy condition (Silva et al., 2019) or neglected (Dolara et al., 2013) but to the detriment of lower performance. Therefore, in this paper, these coefficients will not be neglected and determined following the standard routine, i.e., via the simulation under healthy condition.

- New Method 2 (NewM2):

In fact, as it will be shown later, M1 and M2 do not perform well under all the tested faulty conditions. Thus, a new method denoted NewM2 is proposed. It uses the same formula as M2 for current correction. But for the voltage correction, the term 'V_{OC1}' in (4) is replaced by '$V_{OC1}[1 + \beta_{rel}(25 - T_1)]$'. The reason for this change will be explained in Section 3.2.1 while analyzing the correction performance. Therefore, the equations for NewM2 are:

$$I_2 = I_1\big(1 + \alpha_{rel}(T_{m2} - T_{m1})\big)G_2/G_1 \qquad (5)$$

$$V_2 = V_1 + V_{OC1}[\mathbf{1} + \boldsymbol{\beta_{rel}}(\mathbf{25} - \boldsymbol{T_1})][\beta_{rel}(T_{m2} - T_{m1}) + a \cdot ln(G_2/G_1)] - R_s(I_2 - I_1) - \kappa \cdot I_2(T_{m2} - T_{m1}) \qquad (6)$$

- Method 3 (M3):

Different from M1, M2 or the NewM2, M3 is free from correction coefficient but needs an interpolation constant γ:

$$I_3 = I_1 + \gamma(I_2 - I_1) \qquad (7)$$

$$V_3 = V_1 + \gamma(V_2 - V_1) \qquad (8)$$

According to (IEC 60891, 2009), M3 requires at least 2 reference curves to obtain one corrected curve at specified G or Tm by calculating γ using (7) or (8). Thus, to correct a curve with a requirement on both G and Tm, three curves are necessary.

$$G_3 = G_1 + \gamma(G_2 - G_1) \qquad (9)$$

$$T_3 = T_1 + \gamma(T_2 - T_1) \qquad (10)$$

In summary, the implementation of M1, M2, and NewM2 only requires one single I-V curve, while M3 requires multiple curves. Since their correction procedures are different, their evaluation performance will be conducted separately (in Sections 3 and Section 4, respectively). Since STC (G =1000 W/m^2 and Tm =25 °C) is more commonly adopted as the target condition for I-V curve-based diagnosis, in the following, if not stated, the correction of I-V curves refers to the correction to STC.

2.3. Performance evaluation metrics

The evaluation of correction performance will be conducted from two aspects, i.e., from the whole I-V curve and single extracted parameters (e.g., maximum power P_m, V_{OC} and I_{SC}). Firstly, for the whole I-V curve, the curve error (CE) is adopted as the metric, calculated by the normalized root-mean-square error between the corrected curve and the one

144 simulated-at-STC (from now on called real curve). It should be noted that the real curve only means that *G* and *Tm* are at
145 STC, but the array condition could be either healthy or faulty.

146
$$CE = \frac{\sqrt{\frac{1}{N}\sum_{i=1}^{N}(I_i^c - I_i^{real})^2}}{I_{SC}^{real}} \times 100 \%$$
(11)

147 where, I_i^c and I_i^{real} are the current values from the corrected and actual curve, respectively, for the same voltage V_i. V_i
148 is the ith element of the voltage vector consisting of N points linearly distributed in the interval between 0 and V_{max} with a
149 constant step (V_{max} is constant for all the conditions). The value of V_{max} can be set higher than Voc in order to prevent
150 the voltage after correction from exceeding the set value. In this study, V_{max} is set as 120V and N at 100. I_{SC}^{real} refers
151 to the I_{SC} extracted from the real curve.

152 Then, regarding the parameters, the correction is evaluated with the relative error (*RE*):

153
$$RE_X = \frac{X^c - X^{real}}{X^{real}} \times 100 \%$$
(12)

154 where, X^c and X^{real} are the parameters from the corrected and real curve, respectively. X can be a data coming directly
155 from the curve (such as P_m, V_{OC} or I_{SC}) or one of the parameters of the single-diode model (R_s or R_{sh} for example)
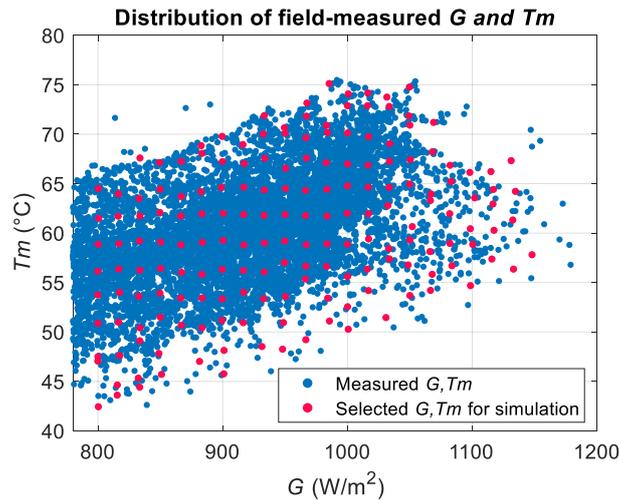156 whose evolution can be considered as a signature of a defect.

157

3. Performance of correction methods using single I-V curve

159 This section focuses on the correction methods based on a single I-V curve, i.e., M1, M2 and NewM2. Firstly, the selection
160 of *G* and *Tm* to generate the curves is presented in Section 3.1. Then, the correction performance (using the metrics *CE*,
161 and *RE*) will be evaluated using the curves simulated under constant or variable fault severity, presented in sections 3.2
162 and 3.3, respectively.

3.1. Selection of *G* and *Tm* based on field measurement

164 To evaluate the correction methods with real environmental conditions, the selection of *G* and *Tm* to generate the curves is
165 based on field measurement (in SIRTA meteorological and climate observatory (Migan et al., 2015), France) of one mc-Si
166 PV module (identical to those used in the simulation in Section 2.1.1) during summer as illustrated in Fig. 2. To minimize
167 the correction error, commonly, the curves' irradiance for correction is selected in the highest range (Ding et al., 2014).
168 Therefore, in our case studies, the lower bound of *G* is set as 800 W/m².

169

170 Fig. 2 Selected *G* and *Tm* based on field-measurement during summer for one mc-Si PV module

171 In Fig. 2, the blue points represent the measured *G* and *Tm,* while the red ones are selected for the simulation. A group of
172 174 pairs of *G* and *Tm* is selected based on a quasi-uniform distribution within the area enclosed by the blue points.

3.2. Correction performance using curves for defects of constant severity

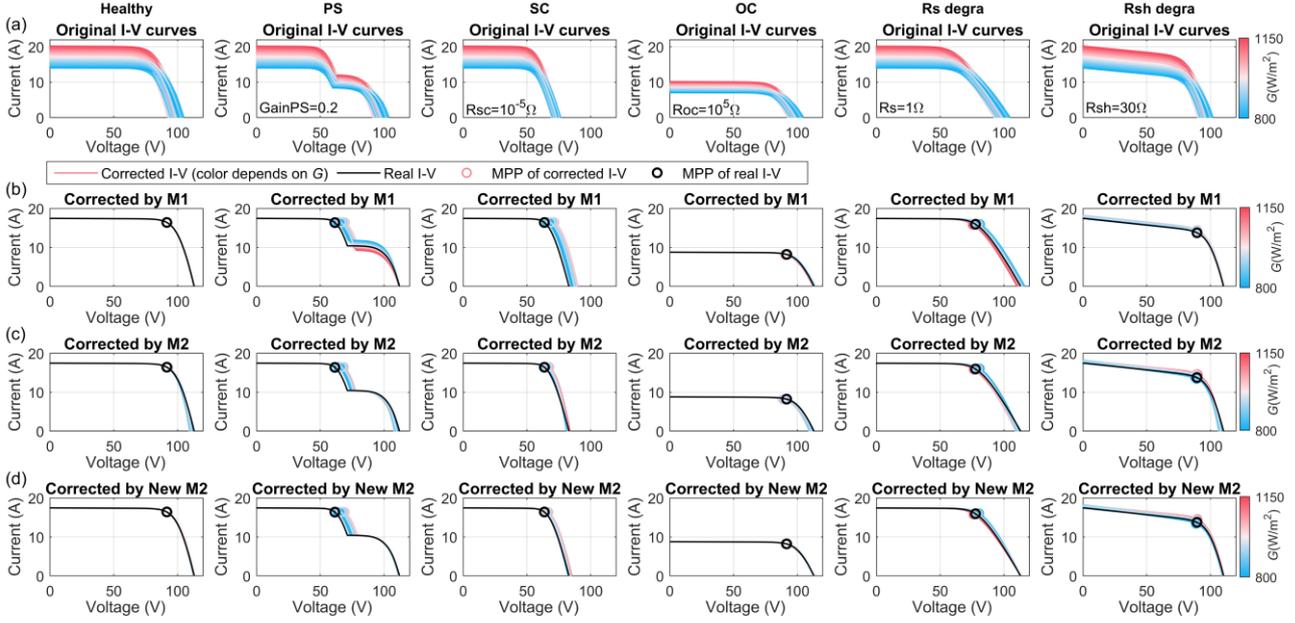174 The fault severity is firstly set constant to investigate the impact of the selected *G* and *Tm*:

175   1) GainPS = 0.2 for partial shading,

176   2)   Rs_degra = 1 Ω for series resistance degradation,

177   3)   Rsh_degra = 30 Ω for shunt resistance degradation

178 Based on the generated curves, the correction performance can now be evaluated. Section 3.2.1 examines the shape of the
179 corrected curves. Section 3.2.2 analyzes the performance evaluation metrics *CE* and *RE* for key curve parameters, and
180 Section 3.2.3 studies the *RE* for the fault features.

181 **3.2.1. Corrected I-V curve form**

182 Using M1, M2 and NewM2, the curves before and after correction are displayed in Fig. 3.

183

184 Fig. 3 Correction results, (a): curves simulated for correction (each condition contains 174 curves with field-measured combinations of
185   *G* and *Tm* at constant fault severity), (b): corrected curves using M1, (c): corrected curves using M2, (d): corrected curves using
186   NewM2 (the displayed color of each curve is determined by the irradiance value with the colorbar on the right side of the figure, the
187   circles on the curves represent the MPP)

188 For the corrected curves, apparent deviations to the real I-V curve can be observed for most faulty conditions using the
189 three methods. These deviations are due to the combined effect of voltage and current corrections, reflected along the *x*
190 *and y* axes, respectively. They are now analyzed as follows:

191 1)   Voltage correction:

192 The deviations due to voltage corrections are observable in all the cases when using M2, but only for SC and Rs degradation
193 when using M1, and for SC when using the NewM2. To analyze these results, we rearrange the voltage correction formulas
194 (2), (4), and (6) as it follows:

195 $$V_2 = k_1 \cdot V_1 + k_2 \cdot (T_{m_2} - T_{m1}) + k_3 \cdot ln(G_2/G_1) + k_4 \cdot (I_2 - I_1) + k_5 \cdot I_2 \cdot (T_{m_2} - T_{m1}), \qquad (13)$$

196 where the different coefficients k_i $(i = 1, \dots, 5)$ for each method, are given in Table 3.

197 <div align="center">Table 3 Coefficients for voltage correction in M1, M2 and NewM2</div>

Method	k_1	k_2	k_3	k_4	k_5
M1	1	$\beta_{rel} \cdot V_{OC}^{STC}$	0	$-R_s$	$-k$
M2	1	$\beta_{rel} \cdot V_{OC1}$	$a \cdot V_{OC1}$	$-R_s$	$-k$
NewM2	1	$\beta_{rel} \cdot V_{OC1} \cdot$ $[1 + \beta_{rel}(T_{m2}^* - T_{m1})]$	$a \cdot V_{OC1}$	$-R_s$	$-k$

198 <div align="center">* In this study, we correct the curves to STC, thus T_{m2} =25 °C</div>

199 Firstly, we compare M1 and M2. Based on the tuning procedure in the standard IEC 60891, k_4 and k_5 are similar for the
200 two methods. As for k_3, it is 0 in M1. In M2, since both the coefficient a and '$ln(G_2/G_1)$' are small values, their product
201 is a second-order term, and its contribution is negligible (within ±0.3 %). As a consequence, the main difference between
202 M1 and M2 lies in k_2. It is noteworthy that k_2 for M1 is constant, while for M2, it depends on V_{OC1} (V_{OC} of the curve
203 to correct). In Fig. 3 (b), there is almost no distortion of the corrected curves when using M1 under healthy condition, which
204 demonstrates the voltage's correction efficiency. As for M2, since T_m of the curves to correct (T_{m1}) are all higher than

205 the target T_m (T_{m2}, 25°C), V_{oc1} is thus always lower than V_{OC}^{STC} (impact of G on V_{OC1} is negligible compared to Tm).
206 Accordingly, $k_2 \cdot (T_{m2} - T_{m1})$ in M2 is lower than in M1. Therefore, the corrected voltage in M2 is lower than in M1.
207 That is the reason why in Fig. 3 (c), we can observe the slight distortions of the corrected curves shifted on the left side of
208 the real curve round the open-circuit point.

209 Besides, the significant correction error under SC and PS for M1 and M2 also originates from the setting of k_2. For SC, to
210 be specific, short-circuit is introduced in one module of one string. As a consequence, V_{OC}^{real} is different from V_{OC}^{STC} (value
211 extracted from the datasheet, i.e., in healthy case), and is equal to around 2/3 of V_{OC}^{STC}. Therefore, in M1, the corrected
212 voltage is higher than the real value. As for M2, V_{OC1}, although varying with Tm, is still closer to V_{OC}^{real}. Consequently,
213 voltage correction is more efficient with M2. Regarding PS (1 module shaded), during the process of I-V scan, when the
214 bypass diodes get activated, the shaded module can be considered as a SC. That explains why a similar deviation is also
215 observed near the inflexion point.

216 From the above analysis, M1 and M2 have their pros and cons in voltage correction. Accordingly, NewM2 is designed by
217 combining their advantages. As observed before, in k_2, using V_{OC}^{STC} (like in M1) could generally lead to better voltage
218 correction than using V_{OC1} (like in M2) except under SC. The exception is because V_{OC}^{STC} fails to reflect V_{OC}^{real}. Therefore,
219 in NewM2, V_{OC1} is replaced by $V_{OC1} \cdot [1 + \beta_{rel}(T_{m2} - T_{m1})]$, which corrects the measured V_{OC1} to the V_{OC} under STC
220 of the real curve and therefore, could better approximate V_{OC}^{real} under any condition. In this way, as shown in Fig. 3 (d),
221 the correction errors near the open-circuit point using M1 (under SC) and using M2 (under other cases) are attenuated.

222 2) Current correction:

223 For the current of corrected curves, noticeable dispersion along the *y*-axis is observed under PS near the inflexion point
224 using M1. In fact, the output current of the PV module is mainly affected by G, while the impact of Tm is limited. Therefore,
225 to analyze this phenomenon, for simplification, the contribution of '$(T_{m2} - T_{m1})$' is neglected. Then we can derive from
226 (1) and (3):

227 • For M1:
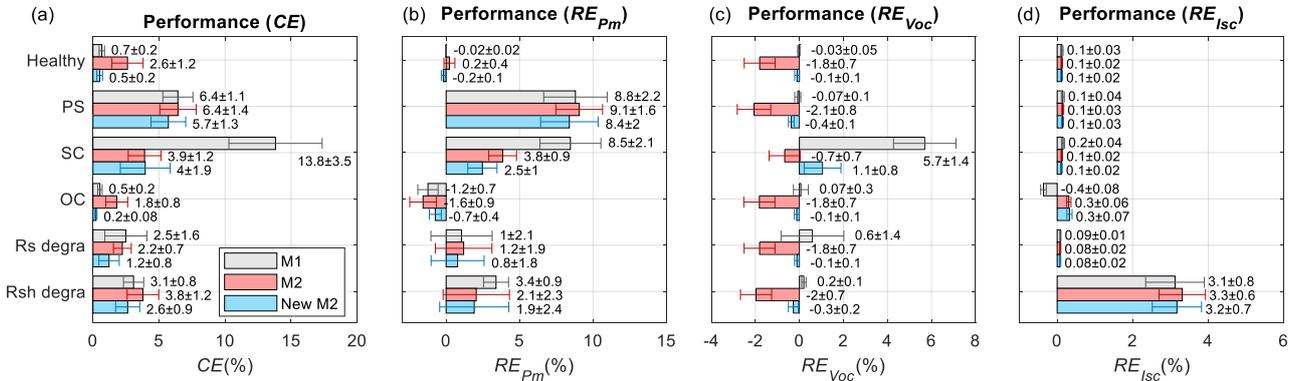
228
$$I_2 = I_1 + I_{SC1}(G_2/G_1 - 1) \tag{14}$$

229 • For M2:

230
$$I_2 = I_1 \cdot G_2/G_1 \tag{15}$$

231 Comparing these two expressions, for M2, the corrected current (I_2) is proportional to the current to correct (I_1). While for
232 M1, there is always a bias that degrades correction's performance, particularly around the inflexion point, like in Fig. 3 (b)
233 under PS. Therefore, M2 performs relatively better than M1 in current correction. That also explains why, for NewM2, the
234 current formula of M2 is chosen, and the same performance is achieved in Fig. 3 (d).

235 **3.2.2. *CE* and *RE* of key curve parameters**

236 Based on the corrected curves, the performance evaluation metrics (*CE*, RE_{P_m}, $RE_{V_{OC}}$ and $RE_{I_{SC}}$) are calculated.
237 Considering that G and Tm are both varying for the 174 curves to correct, the statistics of the metrics are presented in Fig.
238 4.

239

240 Fig. 4 Four metrics to present the correction performance of M1, M2 and NewM2: (a) *CE*, (b) *RE* of P_m, (c) *RE* of V_{oc}, (d) *RE* of
241 I_{SC} (the bars represent the mean value for the correction of 174 curves, while the horizontal whiskers represent the standard deviation
242 (std), these 2 values are marked as 'mean'±'std')

243 These metrics are analyzed as follows:

244 1) *CE*: The value of *CE*, which reflects the correction error on the whole curve, corresponds to the observations in
245   Fig. 3. As expected, high *CE* is found under SC using M1, and PS using all the methods. None of M1 and M2
246   outperforms in all the conditions, but the proposed NewM2 performs better with generally lower and more stable
247   *CE*. The overall average *CE* (2.37 %) decreased by 31.3 % compared to the average when using M2 (3.45 %);

248 2) RE_{P_m}: Similarly, NewM2 performs better correction of P_m. However, it should be noticed that RE_{P_m} is positive
249   under nearly all the conditions for all the methods. This indicates that the fault impact on P_m is underestimated.
250   The mean maximum value is up to 9.1 %, which could hinder the detection of incipient PV fault if P_m is used as
251   a fault indicator;

252 3) $RE_{V_{OC}}$: The results are consistent with our previous observations, i.e., the corrected V_{OC} with M2 is always lower
253   than the real value under all conditions, while the V_{OC} using M1 is relatively better corrected except under SC,
254   where the maximum value of the mean $RE_{V_{OC}}$ could reach 5.7 %. And NewM2 effectively reduces $RE_{V_{OC}}$
255   compared with M1 (in SC), and M2 (in other cases);

256 4) $RE_{I_{SC}}$: The performance of the three methods is similar. It should be noted that, based on (2) and (4), the voltage
257   of the short-circuit point on the original curve (i.e., equals 0), after correction, is positive. This phenomenon is
258   also observed in (Bühler et al., 2014). Therefore, to retrieve the I_{SC} (according to the definition, the
259   corresponding voltage should be 0), the corrected curve must be extrapolated. Here, the extrapolation method in
260   (Bühler et al., 2014) is adopted. In this way, although the current value corrected from the original I_{SC} (I_{SC1}) is
261   close to the actual I_{SC}, there is still a difference that depends on the initial slope of the corrected curve. Indeed for
262   all the conditions except Rsh degradation, where the slope is mild, $RE_{I_{SC}}$ is low (within ±0.5 %). But for Rsh
263   degradation, where the current at MPP is severely lowered down, the slope is steep, and $RE_{I_{SC}}$ is larger.

264 ### 3.2.3. *RE* of fault features

265 Now, we evaluate the correction performance from one or two typical curve parameters, selected as follows:

266 1) PS: The voltage and current at the inflexion point, named V_{rp} and I_{rp} respectively. I_{rp} could reflect the
267   shading level, and V_{rp} the number of activated bypass diodes of PV modules in one string;

268 2) SC: The open-circuit voltage V_{OC};

269 3) OC: The short-circuit current I_{SC};

270 4) Rs degradation: The extracted R_s from I-V curve, $R_s = -\dfrac{1}{\frac{dI}{dV}\big|_{V=V_{OC}}}$ (Chin et al., 2015);

271 5) Rsh degradation: The extracted R_{sh} from I-V curve, $R_{sh} = -\dfrac{1}{\frac{dI}{dV}\big|_{I=I_{SC}}}$ (Chin et al., 2015);

272 For each fault feature, the *RE* is calculated from the values obtained from the corrected and real curves. The results are
273 summarized in Table 4. We can observe large misestimation (absolute mean *RE* >2 %) with V_{rp}, I_{rp}, V_{OC} and R_s when
274 using M1, and V_{rp}, R_s and R_{sh} when using M2 and NewM2. Worse yet, nearly all these large errors (except R_{sh} using
275 M2 and NewM2) lead to underestimating fault features, which will affect the detection of incipient faults. Similarly, none
276 of the three methods outperforms for all the fault features. However, the overall performance of NewM2 is relatively better.

277 Table 4 Impact of correction on fault features using M1, M2 and NewM2

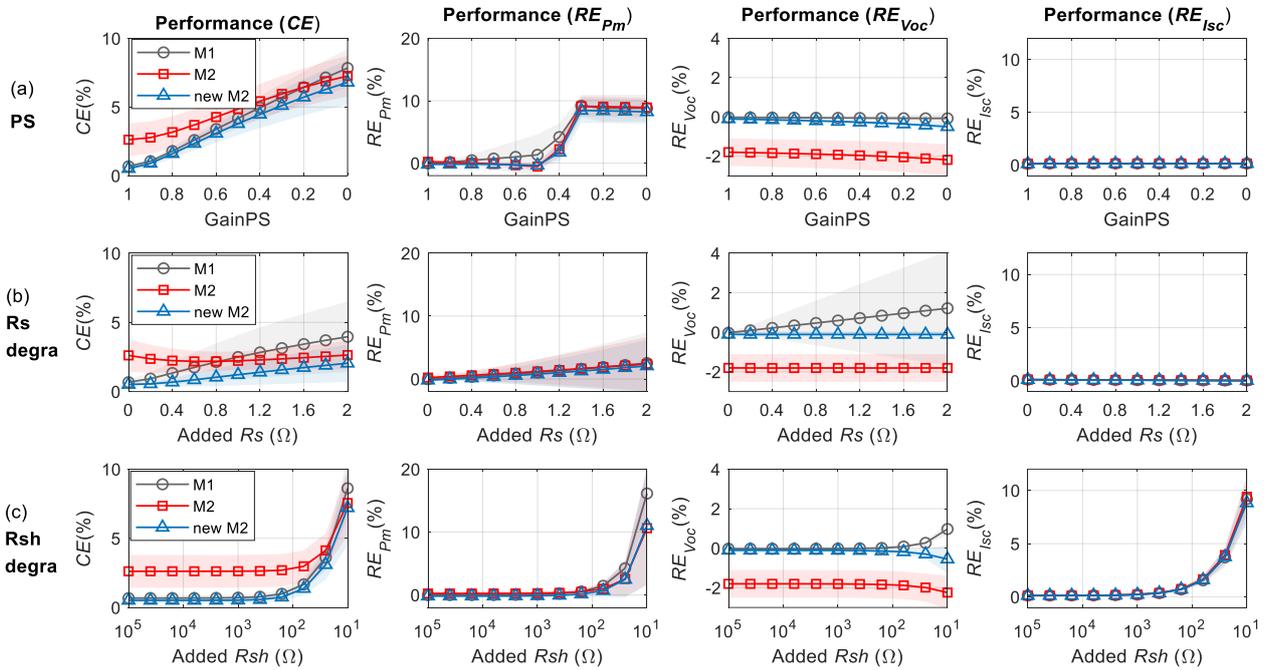| Case	Fault feature	M1		M2		NewM2	
		Value (%) (mean ± std)	Impact on fault feature	Value (%) (mean ± std)	Impact on fault feature	Value (%) (mean ± std)	Impact on fault feature
PS	$RE_{V_{rp}}$	7.3±2.6	Underestimated	6.8±1.3	Underestimated	7.4±1.8	Underestimated
	$RE_{I_{rp}}$	2.5±6.6	Underestimated	-0.2±0.1	Overestimated	-0.2±0.1	Overestimated
SC	$RE_{V_{OC}}$	5.7±1.4	Underestimated	-0.7±0.7	Overestimated	1.1±0.8	Underestimated
OC	$RE_{I_{SC}}$	-0.4±0.08	Overestimated	0.3±0.06	Underestimated	0.3±0.07	Underestimated
Rs degra	RE_{R_s}	-3.4±0.7	Underestimated	-13.6±5.1	Underestimated	-5.5±5.3	Underestimated
Rsh degra	$RE_{R_{sh}}$	-0.1±0.4	Overestimated	-4.6±9.0	Overestimated	-4.1±9.1	Overestimated

278

279 ## 3.3. Correction performance using curves for defects of variable severity

280 In this subsection, the impact of each fault severity on correction performance is investigated. The severities of PS, Rs, and
281 Rsh degradations are varied in the following ranges one at a time: GainPS = 0:0.1:1, R_s_degra =10^{-5}:0.2:2 Ω or R_{sh}_degra

282 $=10^{1:1:5}$ Ω. For each fault level, the curves are simulated for the selected 174 pairs of *G* and *Tm* (presented in Section 3.1),
283 and corrected using the three single-curve based methods.
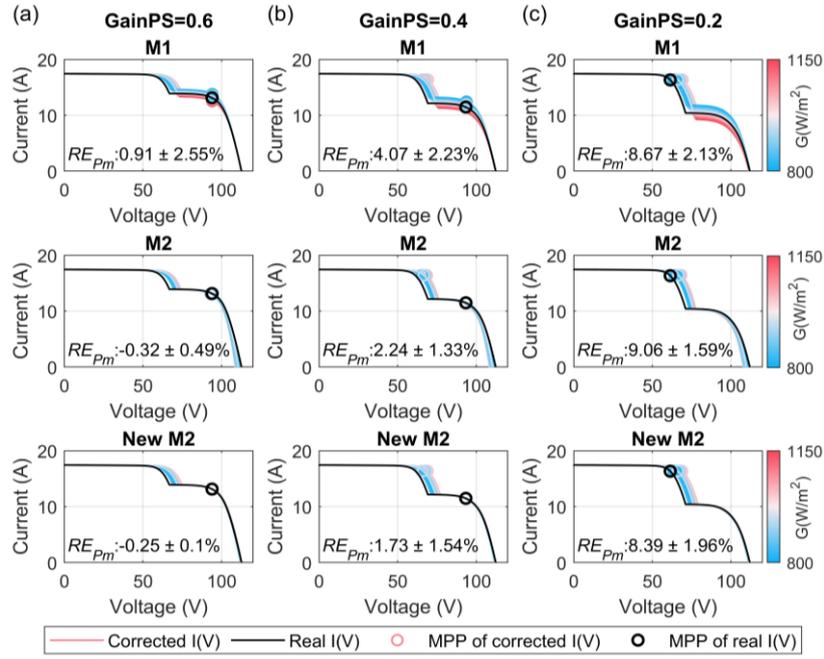
3.3.1. *CE* and *RE* of key curve parameters

285 The performance metrics extracted from these corrected curves are now presented in Fig. 5 as a function of fault severity.

286
287 Fig. 5 *CE* and *RE* of *Pm*, *Voc* and *Isc* using M1, M2 and NewM2 under 3 faulty conditions with variable fault severity: (a) PS, (b) Rs
288 degradation, (c) Rsh degradation (the marked line represents the mean of 174 values obtained from the correction of 174 under each
289 fault severity, while the band area behind represents the standard deviation; the *x*-axis for Rsh degradation is set as log scale; the
290 degree of severity is presented from healthy to severe on the *x*-axis from left to right)

291 From Fig. 5, several remarks can be drawn:

292 • All the metrics have a monotonic variation with the fault severities;

293 • *CE* is mainly sensitive to PS and severe Rsh degradation;

294 • RE_{Pm} is more sensitive to severe Rsh degradation and PS. The step variation observed for PS is due to the
295 maximum power point (MPP) shifting as it can be observed in Fig. 6;

296 • RE_{Voc} and RE_{Isc} are almost insensitive to all faults regardless of their level of severity, except for RE_{Isc} under
297 severe Rs degradation;

298 • The overall performance of NewM2 is better than M1 and M2 with relatively lower *CE* and *RE* for key curve
299 parameters.

Fig. 6 Corrected curves and RE_{P_m} using M1, M2 and NewM2 under three fault severities of PS: (a) GainPS = 0.6, (b) GainPS = 0.4, (c) GainPS = 0.2 (the displayed color of corrected curves and MPP depends on the G of the curve to correct, the circles on the curves represent the MPP, RE_{P_m} are marked as 'mean'±'std')
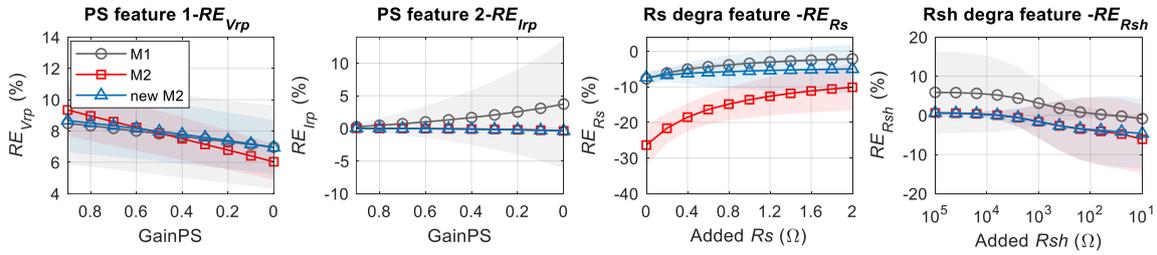
Moreover, it should be noted that, for P_m, which serves as an essential indicator for PV devices' health status, its RE is always positive and gradually increases with the fault severity. This means that using M1 or M2 leads to an inevitable underestimation of the fault impact, which increases with the fault severity.

3.3.2. *RE* of fault features

The impact of fault severity on fault features is also investigated, as illustrated in Fig. 7.

Fig. 7 RE of fault features under PS, Rs and Rsh degradations with variable fault severity (the marked line represents the mean of 174 values obtained from the correction of 174 curves under each fault severity, while the band area behind represents the standard deviation; the x-axis for Rsh degradation is set as log scale; the degree of severity is presented from healthy (except for V_{rp} and I_{rp} as these features do not exist under healthy condition) to severe on the x-axis from left to right)

Concerning the variation of the defect characteristics, different trends are observed: for the features V_{rp} and R_s using all the three methods and for R_{sh} using M1, the RE decreases as the severity of the defect increases. The opposite trend is observed for the other cases. This is due to the different changing rates of each feature's absolute error and its reference value, as defined in (12). Overall, NewM2 performs relatively better with lower and more stable RE.

It should be noted that within the range of severity of the defects tested; all characteristics are underestimated with the three methods. Therefore, used as defect signatures (R_s or R_{sh}, for example), which is typical for PV module degradation analyses, this could hamper the detection and diagnosis of these defects.

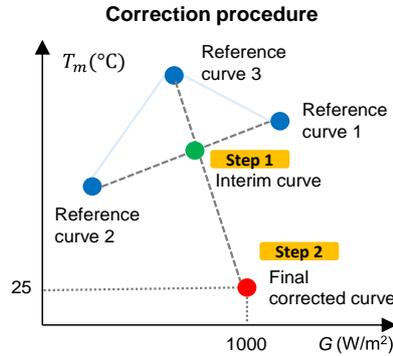## 4. Performance of correction methods using multiple I-V curves

In this section, the method based on multiple curves (M3) will be evaluated. Section 4.1 presents the selection of G and Tm for the reference curves. Sections 4.2 and 4.3 present the correction performance using simulated curves with the selected G and Tm, for constant and then variable fault severity.
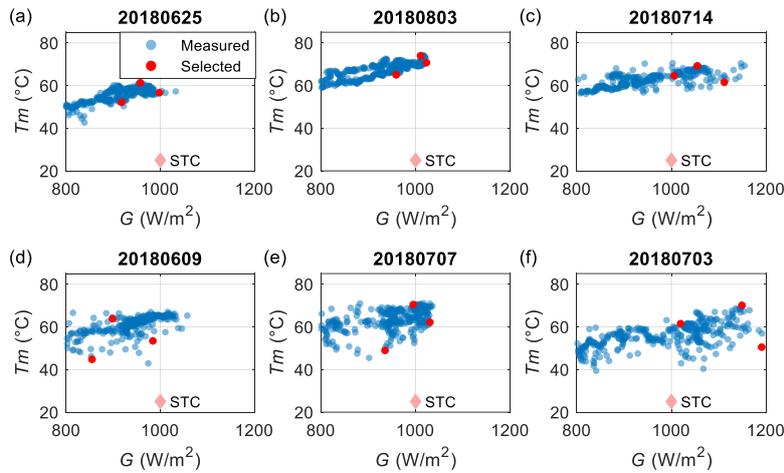
4.1. Selection of *G* and *Tm* for reference curves

Different from M1 and M2, M3 needs at least three reference curves to complete one correction to STC. In this study, like other common applications of M3, we apply the 2-step correction methodology proposed in (IEC 60891, 2009) with three curves. An illustration of this methodology on *G-Tm* plot is shown in Fig. 8.

Fig. 8 Illustration of 2-step correction methodology based on three curves (Step 1: use reference curves 1 and 2 to generate the interim curve; Step 2: use reference curve 3 and the interim curve to get the final corrected curve)

Before the simulation of these curves, *G* and *Tm* need to be determined. The field-measured distributions of *G* and *Tm* of the same mc-Si module employed in the simulation represent as many real situations as possible. As shown in Fig. 8, three reference curves form one group of curves to get one corrected-to-STC curve. The irradiance *G* and temperature *Tm* of these reference curves are determined by one-day measurement, covering sunny and cloudy conditions. The latter have larger fluctuations of *Tm*. Besides, for sunny and cloudy conditions, three possible conditions are also considered for the irradiance: 1) lower than 1000 W/m^2, 2) around 1000 W/m^2 and 3) higher than 1000 W/m^2. In total, 120 groups of *G* and *Tm* are manually selected. Some examples are shown in Fig. 9.

Fig. 9 Examples of selected *G* and *Tm* from different summer days: (a, b, c) clear sunny days, (d, e, f) cloudy days ((a, d): the 3 selected *G* <1000 W/m^2, (b, e): selected *G* around 1000 W/m^2, (c, f): selected *G* > 1000 W/m^2)

4.2. Correction performance using field-measured *G* and *Tm* for defect of constant fault severity

Firstly, we use the same fault configuration presented in Section 3.1 and simulate 120 groups of reference curves regarding the fault severity setting. Then, M3 is applied to obtain 120 corrected curves, as shown in Fig. 10. The corresponding performance metrics and fault features are summarized in Table 5.
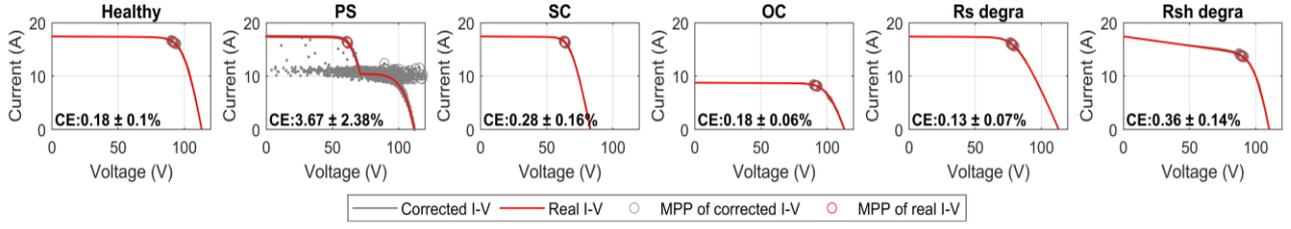
349

350 Fig. 10 Corrected curves using M3 (for PS, due to the large fluctuations, the corrected curves are plotted with dot line for better
351 presentation)

352

353 Table 4 Four metrics to present the correction performance and the impact of correction on fault features using M3

Case	CE (%) (mean ± std)	RE_{P_m}(%) (mean ± std)	$RE_{V_{OC}}$(%) (mean ± std)	$RE_{I_{SC}}$(%) (mean ± std)	Fault feature		
					Feature	Value (%) (mean ± std)	Impact on fault feature
Healthy	0.18±0.10	-0.02±0.1	0.07±0.04	6.10⁻³±0.05	-	-	-
PS	3.67±2.38	7.5±18.3	0.06±0.07	6.10⁻³±0.05	$RE_{V_{rp}}$	-6.9±32.0	Overestimated
					$RE_{I_{rp}}$	3.2±12.2	Underestimated
SC	0.28±0.16	0.03±0.3	0.2±0.1	6.10⁻³±0.05	$RE_{V_{OC}}$	0.2±0.1	Underestimated
OC	0.18±0.06	2e-4±0.2	0.07±0.05	6.10⁻³±0.05	$RE_{I_{SC}}$	6.10⁻³±0.05	Underestimated
Rs degra	0.13±0.07	0.1±0.2	0.07±0.03	6.10⁻³±0.05	RE_{R_s}	0.01±0.04	Overestimated
Rsh degra	0.36±0.14	0.4±0.2	0.05±0.04	6.10⁻³±0.05	$RE_{R_{sh}}$	4.10⁻³±0.01	Underestimated

354

355 From the results, clearly, except for PS, M3 achieves good correction (mean value of all metrics within ±1 %) for all the
356 conditions.

357 In the following, we analyze the 'catastrophic' correction error near the inflexion point under PS. As illustrated in Fig. 8,
358 the correction procedure using M3 is done in two steps. An example of these steps under PS is shown in Fig. 11. In step 1,
359 due to the unsynchronized appearance of inflexion points on reference curves 1 and 2 (i.e., V_{rp} are not identical), another
360 inflexion point is created on the intermediate curve, so that in step 2, a strange curve shape is introduced. This phenomenon
361 could lead to a large error on P_m but with no significant impact on V_{oc} and I_{SC}.
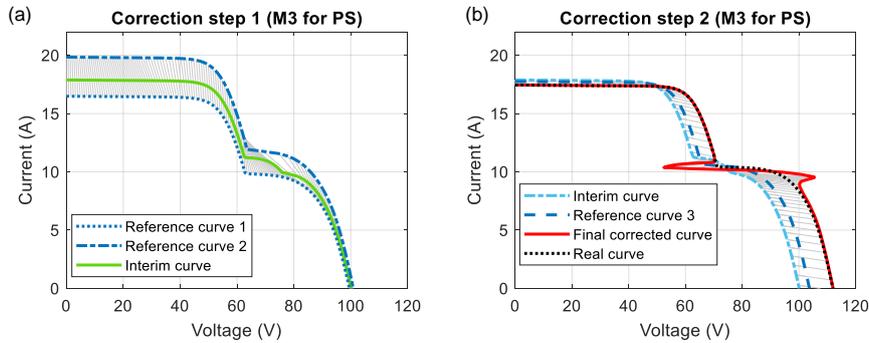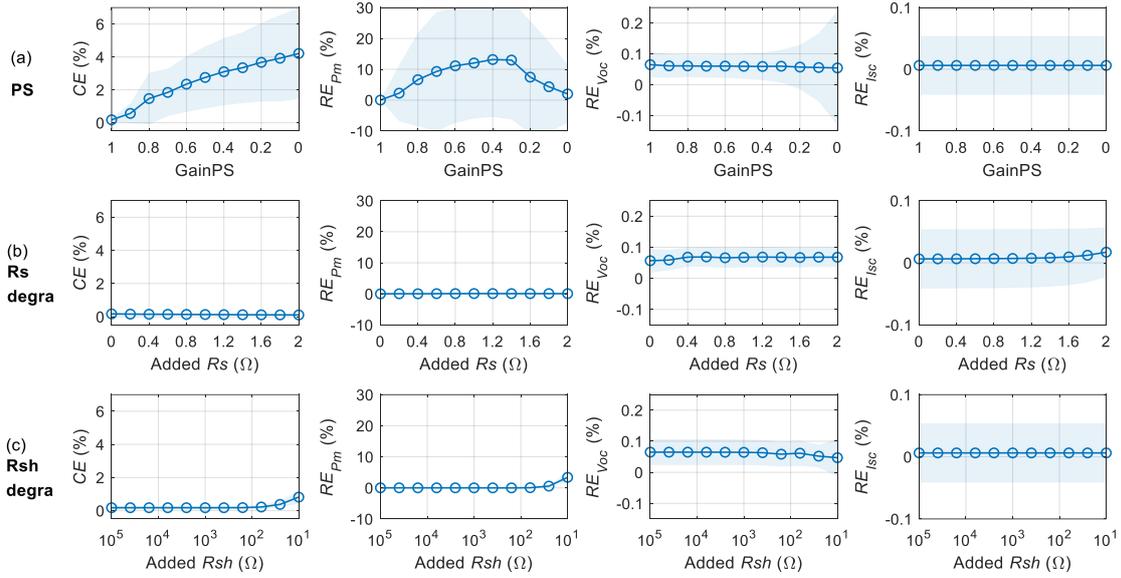

362

363 Fig. 11 Correction procedure under PS using 3 reference curves-based M3: (a) correction step 1, (b) correction step 2

364 Also, it should be noted that the fault impact on all the fault features is underestimated. Furthermore, as expected, the most
365 significant error occurs under PS. Under the other conditions, the *RE* is within ±1 %.

4.3. Correction performance using field-measured *G* and *Tm* for defects of variable severity

367 In this subsection, the impact of fault severity on correction performance using M3 is investigated. The severity for PS, Rs
368 and Rsh degradations is varied using the same setting as in Section 3.2. The performance metrics as a function of fault
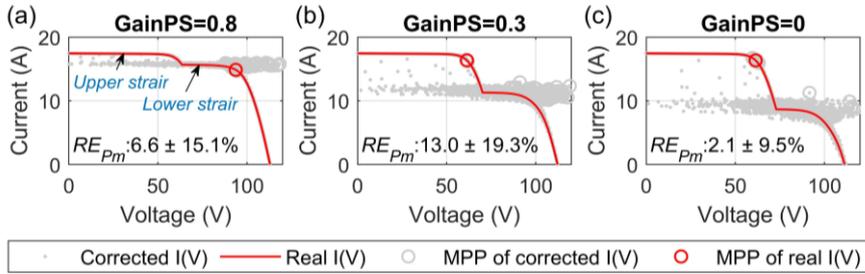369 severity are presented in Fig. 12.

Fig. 12 *CE* and *RE* of *Pm*, *Voc* and *Isc* for M3 under 3 faulty cases with variable fault severity: (a) PS, (b) Rs degradation, (c) Rsh degradation (the circled line represents the mean value for the 120 corrected curves for each fault severity, while the band area behind represents the standard deviation; the *x*-axis for Rsh degradation is set as log scale; the degree of severity is presented from healthy to severe on the *x*-axis from left to right)

From these results, the following remarks could be drawn:

- Regarding Rs and Rsh degradations, all the metrics are insensitive to the fault level;

- Regarding PS, only *CE* and RE_{Pm} vary according to the fault severity. *CE* has a monotonic variation, which makes it relevant for fault severity estimation. However, RE_{Pm} is not a reliable feature as it exhibits a non-monotonic variation. This phenomenon is due to the displacement of the maximum power point (MPP) as illustrated in Fig. 13.
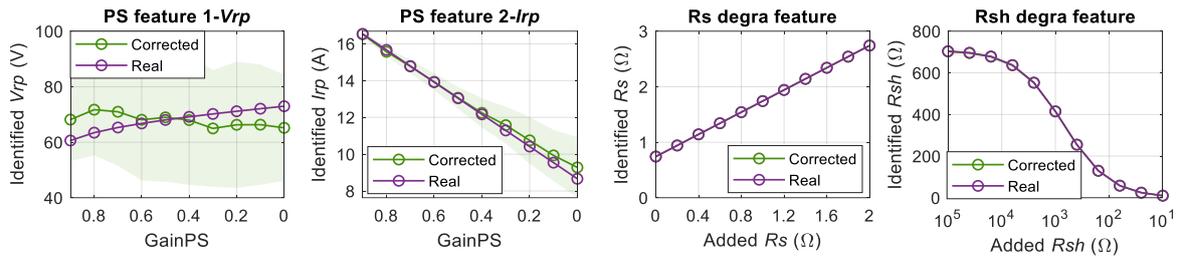

Fig. 13 Corrected curves using M3 under 3 fault severities of PS: (a) GainPS=0.8, where MPP of real and corrected curves are all at 'lower stair', (b) GainPS = 0.3, where MPP of real is at 'upper stair' while MPP of most corrected curves at 'lower stair' (c) GainPS = 0, MPP of real and most corrected curves are all at 'upper stair' (for each case, RE_{Pm} is marked as 'mean'±'std')

The behavior of fault features is also investigated with the comparison of identified features from both corrected and real I-V curves presented in Fig. 14 and the corresponding relative errors (*RE*) in Fig. 15.
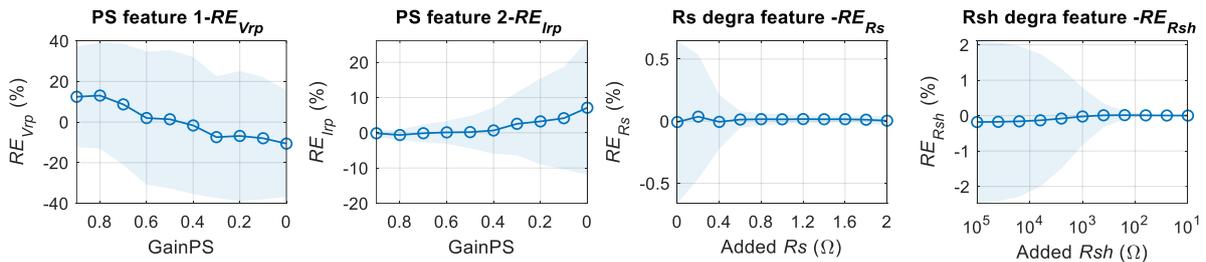
390

Fig. 14 Identified feature from corrected (using M3) and original I-V curve for fault of variable severity (the circled line represents the
mean, while the band area represents the standard deviation; the values of R_s or R_{sh} identified from I-V curve are not equal to the
additional resistance (illustrated in Fig. 1) due to the existence of inherent equivalent R_s (0.74 Ω) or R_{sh} (708.36 Ω) of PV arrays

396

Fig. 15 RE of fault features under PS, Rs and Rsh degradations for fault of variable severity using M3 (the circled line represents the
mean, while the band area represents the standard deviation)

The large dispersion observed for RE_{Vrp} and RE_{Irp} confirms the poor performance of the correction near the inflection
point. The values of R_s and R_{sh} extracted from the original and corrected curves are very close, as confirmed in Fig. 14.
This is also reflected in the low values of RE_{R_s} and $RE_{R_{sh}}$ displayed in Fig. 15. The mean value of RE_{R_s} lies within
±0.1 % and that of $RE_{R_{sh}}$ within ±0.2 %, and both are relatively insensible to the varying fault severity. It is also noted
that the standard deviations of RE_{R_s} and $RE_{R_{sh}}$ exhibit a decreasing trend when the fault severity increases. In all, with
varying fault, M3 achieves quite good and robust correction under Rs and Rsh degradation.

5. Discussion

5.1. Summary of correction methods

The correction performance using three single and one multiple curves-based methods has been evaluated. Each method
has its own pros and cons listed in Table 6.

Table 6 Pros and Cons of correction methods

	Single curve-based methods			Multiple curves-based method (M3)
	M1	M2	NewM2	
Pros	• Better correction of voltage than M2 • Suitable for rapid field diagnosis	• Better correction of current than M1	• Better overall performance than M1 and M2	• High-precision correction performance under most conditions • Free of correction coefficients
Cons	• Needs to determine the correction coefficients • Prone to large underestimation of P_m, and fault features			• Not suitable for rapid field diagnosis • Needs at least 3 well-chosen reference curves • Poor correction near inflexion point under PS with high effect on P_m

Once established (i.e., correction coefficients determined), all these single curve-based correction methods can conduct
rapid correction of measured I-V curves. This allows their integration in real-time health monitoring of PV devices.
However, as discussed in Section 2.2, the determination of correction coefficients is a troublesome task. The coefficients
determined using simulated data do not always fit the real values, especially for the installed PV panels after a long-time
operation. The proposed NewM2, which combines M1 and M2's advantages, leads to better correction performance in all

fault conditions tested. However, it still introduces a significant correction error in the case of partial shading (PS), the degradation of Rs and Rsh, compared to healthy conditions, short circuit (SC) and open circuit (OC).

As for the multiple-curves-based method (M3), except under PS, excellent correction is obtained. However, the selection of reference curves is still a manual process (Hishikawa et al., 2016; IEC 60891, 2009), which could hinder its application in rapid or on-line field correction.

5.2. Suggestions for future work

Based on comparing the three IEC 60891 correction methods and the new proposal, some suggestions on future work are hereafter presented.

For correction methods based on a single curve, the determination of correction coefficients for PV panels on-site remains difficult. A strategy for determining these coefficients based on field measured data needs to be developed that differs from the IEC 60891 procedure, which requires environmental conditions that are only practically feasible in fully equipped laboratories. Solutions to reduce dependence on correction coefficients, such as (Hishikawa et al., 2019, 2018), should also be further developed and validated with I-V curves taken from panels with defects.

The proposed new correction method still needs to be evaluated with more types of defects.

For the correction method based on multiple curves, two improvements are expected. On the one hand, efforts are needed to improve correction performance in case of partial shading; on the other hand, developing a methodology for automatic and efficient selection of reference curves would facilitate the deployment of the technique in the field.

Correction methods should be evaluated with field-measured data.

6. Conclusion

In this work, we have evaluated the performance of methods based on one or more curves proposed in the IEC 60891 standard for the correction of I-V curves measured on defective photovoltaic panels. It has been shown that all the methods introduce significant errors due to irradiance, module temperature and the severity of the defects. Using the standard method M1 of the IEC, we have pointed out that a distortion of the curve's shape is commonly introduced with a relative error up to 13.8%. For P_m and the fault characteristics extracted from the corrected curves, estimation errors also occur frequently. Even worse still, most significant errors result in underestimating the characteristics (up to 9.1% for P_m using M2). This can affect the detection of incipient PV defects if these characteristics are used as defect signatures.

Among the single curve-based methods (M1 and M2), none of them could outperform under all the faulty simulated conditions. Therefore, an M2-based improved method (NewM2) has been proposed. It has exhibited more robust overall performance than M1 and M2 with the decrease of average curve error from 3.45% to 2.37%.

The method based on multiple curves (M3) generally has higher performance than those based on a single curve, but it is not suitable for rapid field diagnosis.

PV health monitoring and fault diagnosis using I-V curves is a promising approach. However, several signs of progress are expected from future work to improve its efficiency and ease its implementation. At first, the determination of correction coefficients based on field-measured data or mitigating the dependence on correction coefficients would be beneficial. Second, the development of a methodology for automatic determination of reference curves and improved correction performance (mainly to avoid underestimating incipient faults) under different faulty conditions.

References

Agrawal, N., Bora, B., Kapoor, A., 2020. Experimental investigations of fault tolerance due to shading in photovoltaic modules with different interconnected solar cell networks. Sol. Energy 211, 1239–1254. https://doi.org/10.1016/j.solener.2020.10.060

Bouaichi, A., Alami, A., Hajjaj, C., Messaoudi, C., Ghennioui, A., Benlarabi, A., Ikken, B., El, A., Zitouni, H., 2019. In-situ evaluation of the early PV module degradation of various technologies under harsh climatic conditions : The case of Morocco. Renew. Energy 143, 1500–1518. https://doi.org/10.1016/j.renene.2019.05.091

465   Bühler, A.J., Perin Gasparin, F., Krenzinger, A., 2014. Post-processing data of measured I–V curves of photovoltaic
466   devices. Renew. Energy 68, 602–610. https://doi.org/10.1016/j.renene.2014.02.048

467   Chen, Z., Wu, L., Cheng, S., Lin, P., Wu, Y., Lin, W., 2017. Intelligent fault diagnosis of photovoltaic arrays based on
468   optimized kernel extreme learning machine and I-V characteristics. Appl. Energy 204, 912–931.
469   https://doi.org/10.1016/j.apenergy.2017.05.034

470   Chin, V.J., Salam, Z., Ishaque, K., 2015. Cell modelling and model parameters estimation techniques for photovoltaic
471   simulator application: A review. Appl. Energy 154, 500–519. https://doi.org/10.1016/j.apenergy.2015.05.035

472   Ding, K., Zhang, J., Bian, X., Xu, J., 2014. A simplified model for photovoltaic modules based on improved translation
473   equations. Sol. Energy 101, 40–52. https://doi.org/10.1016/j.solener.2013.12.016

474   Dolara, A., Lazaroiu, G.C., Leva, S., Manzolini, G., 2013. Experimental investigation of partial shading scenarios on PV
475   (photovoltaic) modules. Energy 55, 466–475. https://doi.org/10.1016/j.energy.2013.04.009

476   Fadhel, S., Delpha, C., Diallo, D., Bahri, I., Migan, A., Trabelsi, M., Mimouni, M.F., 2019. PV shading fault detection
477   and classification based on I-V curve using principal component analysis: Application to isolated PV system. Sol.
478   Energy 179, 1–10. https://doi.org/10.1016/j.solener.2018.12.048

479   Friesen, G., Herrmann, W., Belluardo, G., Herteleer, B., 2018. Report IEA-PVPS T13-11:2018 Photovoltaic module
480   energy yield measurements: Existing approaches and best practice, IEA-PVPS. URL https://iea-pvps.org/wp-
481   content/uploads/2020/01/Photovoltaic_Module_Energy_Yield_Measurements_Existing_Approaches_and_Best_Pr
482   actice_by_Task_13.pdf (accessed 6.15.20).

483   Golive, Y.R., Singh, H.K., Kottantharayil, A., Vasi, J., Shiradkar, N., 2019. Investigation of Accuracy of various STC
484   Correction Procedures for I-V Characteristics of PV Modules Measured at Different Temperature and Irradiances,
485   in: 2019 IEEE 46th Photovoltaic Specialists Conference (PVSC). IEEE, Chicago, IL, USA, pp. 2743–2748.
486   https://doi.org/10.1109/PVSC40753.2019.8980557

487   Hishikawa, Y., Doi, T., Higa, M., Yamagoe, K., Ohshima, H., Takenouchi, T., Yoshita, M., 2018. Voltage-dependent
488   temperature coefficient of the I-V curves of crystalline silicon photovoltaic modules. IEEE J. Photovoltaics 8, 48–
489   53. https://doi.org/10.1109/JPHOTOV.2017.2766529

490   Hishikawa, Y., Ohshima, H., Higa, M., Yamagoe, K., Doi, T., 2016. Precise Determination of the STC I-V Curves by
491   Wide-Range Linear Extrapolation of Outdoor I-V Curves on Partly Sunny Days, in: 32nd European Photovoltaic
492   Solar Energy Conference and Exhibition (Eu-PVSEC). München, Germany, pp. 1716–1719.
493   https://doi.org/10.4229/EUPVSEC20162016-5DO.11.4

494   Hishikawa, Y., Takenouchi, T., Higa, M., Yamagoe, K., Ohshima, H., Yoshita, M., 2019. Translation of Solar Cell
495   Performance for Irradiance and Temperature from a Single I-V Curve Without Advance Information of Translation
496   Parameters. IEEE J. Photovoltaics 9, 1195–1201. https://doi.org/10.1109/JPHOTOV.2019.2924388

497   Huang, J.M., Wai, R.J., Gao, W., 2019. Newly-designed fault diagnostic method for solar photovoltaic generation system
498   based on IV-Curve measurement. IEEE Access 7, 70919–70932. https://doi.org/10.1109/ACCESS.2019.2919337

499   Huawei, 2020. Smart I-V Curve Diagnosis. URL https://solar.huawei.com/en-
500   GB/download?p=%2F-%2Fmedia%2FSolar%2Fattachment%2Fpdf%2Feu%2Fdatasheet%2FIV-Curve.pdf
501   (accessed 8.17.20).

502   IEC 60891, 2009. Photovoltaic devices - Procedures for temperature and irradiance corrections to measured I-V
503   characteristics.

504   Li, Y., Ding, K., Zhang, J., Chen, F., Chen, X., Wu, J., 2019. A fault diagnosis method for photovoltaic arrays based on
505   fault parameters identification. Renew. Energy 143, 52–63. https://doi.org/10.1016/j.renene.2019.04.147

506   Ma, M., Liu, H., Zhang, Z., Yun, P., Liu, F., 2019. Rapid diagnosis of hot spot failure of crystalline silicon PV module
507   based on I-V curve. Microelectron. Reliab. 100–101. https://doi.org/10.1016/j.microrel.2019.113402

508   Martínez-Moreno, F., Figueiredo, G., Lorenzo, E., 2018. In-the-field PID related experiences. Sol. Energy Mater. Sol.

509   Cells 174, 485–493. https://doi.org/10.1016/j.solmat.2017.09.037

510   Mellit, A., Tina, G.M., Kalogirou, S.A., 2018. Fault detection and diagnosis methods for photovoltaic systems: A review.

511   Renew. Sustain. Energy Rev. 91, 1–17. https://doi.org/10.1016/j.rser.2018.03.062

512   Migan, A., Mambrini, T., Bourdin, V., Badosa, J., 2015. Deployment of a multi-technology photovoltaic module test

513   bench on the SIRTA meteorological and climate observatory, in: 31st European PV Solar Energy Conference and

514   Exhibition (Eu-PVSEC). Hamburg, Germany.

515   Pillai, D.S., Rajasekar, N., 2018. A comprehensive review on protection challenges and fault diagnosis in PV systems.

516   Renew. Sustain. Energy Rev. 91, 18–40. https://doi.org/10.1016/j.rser.2018.03.082

517   Rajput, P., Tiwari, G.N., Sastry, O.S., Bora, B., Sharma, V., 2016. Degradation of mono-crystalline photovoltaic modules

518   after 22 years of outdoor exposure in the composite climate of India. Sol. Energy 135, 786–795.

519   https://doi.org/10.1016/j.solener.2016.06.047

520   Sarikh, S., Raoufi, M., Bennouna, A., Benlarabi, A., Ikken, B., 2020. Implementation of a plug and play I-V curve tracer

521   dedicated to characterization and diagnosis of PV modules under real operating conditions. Energy Convers.

522   Manag. 209. https://doi.org/10.1016/j.enconman.2020.112613

523   Silva, A.M., Melo, F.C., Reis, J.H., Freitas, L.C.G., 2019. The study and application of evaluation methods for

524   photovoltaic modules under real operational conditions, in a region of the Brazilian Southeast. Renew. Energy 138,

525   1189–1204. https://doi.org/10.1016/j.renene.2019.01.129

526   Spataru, S., Sera, D., Kerekes, T., Teodorescu, R., 2015. Monitoring and Fault Detection in Photovoltaic Systems Based

527   On Inverter Measured String I-V Curves, in: 31st European Photovoltaic Solar Energy Conference and Exhibition

528   (EU PVSEC). Hamburg, Germany, pp. 1667–1674. https://doi.org/10.4229/EUPVSEC20152015-5BO.12.2

529   Tanesab, J., Parlevliet, D., Whale, J., Urmee, T., 2017. Seasonal effect of dust on the degradation of PV modules

530   performance deployed in different climate areas. Renew. Energy 111, 105–115.

531   https://doi.org/10.1016/j.renene.2017.03.091

532   Tanesab, J., Parlevliet, D., Whale, J., Urmee, T., Pryor, T., 2015. The contribution of dust to performance degradation of

533   PV modules in a temperate climate zone. Sol. Energy 120, 147–157. https://doi.org/10.1016/j.solener.2015.06.052

534   Triki-Lahiani, A., Bennani-Ben Abdelghani, A., Slama-Belkhodja, I., 2018. Fault detection and monitoring systems for

535   photovoltaic installations: A review. Renew. Sustain. Energy Rev. 82, 2680–2692.

536   https://doi.org/10.1016/j.rser.2017.09.101

537   Wang, M., Liu, J., Burleyson, T.J., Schneller, E.J., Davis, K.O., French, R.H., Braid, J.L., 2020. Analytic

538   I_{sc}–V_{oc} Method and Power Loss Modes From Outdoor Time-Series I–V Curves.

539   IEEE J. Photovoltaics 10, 1379–1388. https://doi.org/10.1109/JPHOTOV.2020.2993100

540   Zhu, H., Lu, L., Yao, J., Dai, S., Hu, Y., 2018. Fault diagnosis approach for photovoltaic arrays based on unsupervised

541   sample clustering and probabilistic neural network model. Sol. Energy 176, 395–405.

542   https://doi.org/10.1016/j.solener.2018.10.054

543   Zhu, Y., Xiao, W., 2020. A comprehensive review of topologies for photovoltaic I–V curve tracer. Sol. Energy.

544   https://doi.org/10.1016/j.solener.2019.12.020

545